

# The Proton Gluon Distribution from the Color Dipole Picture

G.R. Boroun

*Department of Physics, Razi University,  
Kermanshah 67149, Iran*

M. Kuroda

*Center for Liberal Arts, Meiji Gakuin University  
Yokohama, Japan*

Dieter Schildknecht

*Fakultät für Physik, Universität Bielefeld  
D-33501 Bielefeld, Germany  
and*

*Max-Planck-Institut für Physik (Werner-Heisenberg-Institut)  
Föhringer Ring 6, D-80805 München, Germany  
(Dated: December 13, 2022)*

Employing the representation of the experimental data on deep inelastic electron-proton scattering (DIS) in the color-dipole picture (CDP), we determine the gluon distribution of the proton at small Bjorken  $x$ . At sufficiently large momentum transfer,  $Q^2$ , the extracted gluon distribution fulfills the evolution equation for the proton structure function. For low values of  $Q^2$ , e.g. for  $Q^2 = 1.9 \text{ GeV}^2$ , the evolution equation for the proton structure function is violated. The standard procedure of adopting a low- $Q^2$  input scale for the extraction of the gluon density is highly questionable.

## I. INTRODUCTION

The extraction of the gluon-distribution function [1–4] of the proton from deep-inelastic electron-proton scattering (DIS) [5] rests on the determination of the fit parameters in an ad-hoc parametrization of the gluon  $x$ -distribution at a low- $Q^2$  input scale.<sup>1</sup> It is well-known, and was recently emphasized [6] that the results on the gluon distribution function from different collaborations [1–4] show a significant spread in the low- $x$ , low- $Q^2$  domain. The quality of the fits is considered [6] not to be satisfactory. This led to the introduction of phenomenological power corrections [7, 8] to the structure functions, and to modifications [6] of the DGLAP evolution equations [9] for the gluon distribution by a non-linear term [10, 11].

Rather than applying ad hoc modifications to the evolution equations at low  $Q^2$ , it seems appropriate to employ a representation of the proton structure functions at low- $x$  that smoothly connects the regions of large- $Q^2$ , where perturbative QCD (pQCD) is expected to be valid, and of low- $Q^2$  via a single dynamical mechanism.

A representation fulfilling this requirement is the color-dipole picture (CDP) [12], [13], [14], [15]. The CDP, originating from Generalized Vector Dominance (GVD) [16],<sup>2</sup> smoothly connects the representation of the proton

structure functions at high  $Q^2$ , dominantly due to scattering of high-mass  $q\bar{q}$  fluctuations<sup>3</sup> of the (virtual) photon, with the representation at low- $Q^2$  due to  $q\bar{q}$  bound states, including  $Q^2 = 0$ , where the interaction is essentially due to the scattering of the low-lying vector mesons  $\rho^0$ ,  $\omega$  and  $\phi$ .

In the present paper, accordingly, the leading order gluon distribution of the perturbative-QCD-improved (pQCD) parton model is extracted from the representation of the proton structure functions  $F_2(x, Q^2)$  and  $F_L(x, Q^2)$  in the CDP. We find that at low  $x$ , for  $Q^2$  sufficiently large ( $Q^2 \gtrsim 10 \text{ GeV}^2$  to  $20 \text{ GeV}^2$ ), the experimental results on DIS parametrised by the CDP fulfill evolution in distinction from low values of  $Q^2$  (e.g. for  $Q^2 = 1.9 \text{ GeV}^2$ ), where due to hadronlike behaviour of DIS, the standard evolution equation is strongly violated. This result suggests that the unsatisfactory fits mentioned in Ref.[6] at low  $Q^2$  are due to an improper use of a low- $Q^2$  input scale, such as  $Q^2 = 1.9 \text{ GeV}^2$ , in the widely employed analysis of the DIS experimental results.

In Section II, we briefly review the determination of the gluon distribution at leading order of  $\alpha_s(Q^2)$  from the pQCD improved parton model. In Section III, we review the relevant parts of the CDP. In Section IV, as an alternative to the CDP, we consider and summarise the Froissart-bounded representation of  $F_2(x, Q^2)$ . In Sec-

<sup>1</sup> In standard notation, the virtuality of the photon is denoted by  $Q^2$ , and  $x$  is the Bjorken scaling variable,  $x \cong Q^2/W^2$ , where  $W$  denotes the virtual-photon-proton center of mass energy.

<sup>2</sup> For a more recent review see ref. [17]

<sup>3</sup> See ref.[18] for a detailed quantitative estimate of the range of masses of  $q\bar{q}$  fluctuation for given  $Q^2 \geq 0$ .

tion V, the results obtained for the gluon distribution are presented for both the CDP and the Froissart-bounded parametrization of the DIS data. At low  $Q^2$  ( $Q^2 = 1.9\text{GeV}^2$ ), we observe drastic differences between our results and the results [6] based on the application of ad hoc modifications of the gluon evolution equations. Note that for the extraction of the gluon distribution in Sections II to V, no use is being made of the pQCD evolution equations [9].

In Sections VI and VII, we examine the consistency between the low- $Q^2$  dependence at low- $x$  of our results for the gluon distribution and the validity of the evolution equation for the structure function  $F_2(x, Q^2)$ . At large  $Q^2$ , specifically for approximately  $20\text{GeV}^2 \lesssim Q^2 \lesssim 100\text{GeV}^2$ , the gluon distribution is consistent with the validity of evolution, leading to the important constraint of  $C_2 = 0.29$  for the exponent in the dependence of  $F_2(x, Q^2)$  on  $(W^2)^{C_2} = (Q^2/x)^{C_2}$ . The predicted value of  $C_2 \cong 0.29$  agrees with experiment. At low- $Q^2$ , the logarithmic derivative of the structure function  $F_2(x, Q^2)$  deviates from the prediction of the evolution equation by a factor of magnitude up to 3. Final Conclusions are presented in Section VIII.

## II. THE DETERMINATION OF THE GLUON DISTRIBUTION FUNCTION IN PQCD.

In the pQCD improved parton model, the longitudinal structure function  $F_L(x, Q^2)$  to lowest order of  $\alpha_s(Q^2)$  is given by [19]

$$F_L(x, Q^2) = \frac{\alpha_s(Q^2)}{4\pi} \left( \frac{16}{3} I_F + 8 \sum Q_q^2 I_g \right), \quad (2.1)$$

where

$$I_F \equiv I_F(x, Q^2) = \int_x^1 \frac{dy}{y} \left( \frac{x}{y} \right)^2 F_2(y, Q^2), \quad (2.2)$$

and

$$I_g \equiv I_g(x, Q^2) = \int_x^1 \frac{dy}{y} \left( \frac{x}{y} \right)^2 \left( 1 - \frac{x}{y} \right) G(x, Q^2), \quad (2.3)$$

the gluon density being denoted by  $G(x, Q^2) = xg(x, Q^2)$ , and  $\sum Q_q^2 = 10/9$  for four flavors of quarks. The term proportional to  $I_F$  in (2.1) is due to  $\gamma^*$ -quark (antiquark) interaction with gluon emission,

$$\gamma^* + q(\bar{q}) \rightarrow q(\bar{q}) + g, \quad (2.4)$$

while the term proportional to  $I_g$  in (2.1) originates from quark-antiquark production,

$$\gamma^* + g \rightarrow q\bar{q}. \quad (2.5)$$

The successful representation of the experimental data on DIS in the CDP is based on incorporating [12] the  $q\bar{q}$ -color-dipole interaction (2.5) with the gluon field of the

proton

$$\begin{aligned} &(\gamma^* \rightarrow q\bar{q}) + g \rightarrow q\bar{q} \\ &\text{or} \\ &\gamma^* + (g \rightarrow q\bar{q}) \rightarrow q\bar{q}, \end{aligned} \quad (2.6)$$

into the mass-dispersion relation of Generalized Vector Dominance (GVD) [16]. In the CDP the photon makes a transition to  $q\bar{q}$  states that interact with gluons, or, equivalently, the photon (exclusively) interacts with the  $q\bar{q}$  sea originating from  $g \rightarrow q\bar{q}$  transitions, see (2.6).

Accordingly, the gluon term associated with reaction (2.5) is the dominant one in the pQCD expression (2.1),

$$F_L(x, Q^2) = \frac{2\alpha_s(Q^2)}{\pi} \sum_q Q_q^2 I_g(x, Q^2). \quad (2.7)$$

In the CDP of low- $x$  DIS, the large- $Q^2$  pQCD equality (2.1) is replaced by (2.7), thus excluding (2.4).

For a wide range of different gluon distributions, independently of their specific form, the evaluation of  $I_g(x, Q^2)$  from (2.3) in (2.7) yields the well-known approximate result [19, 14] for the longitudinal structure function (2.7)

$$F_L(\xi_L x, Q^2) = \frac{\alpha_s(Q^2)}{3\pi} \sum_q Q_q^2 G(x, Q^2). \quad (2.8)$$

A given gluon distribution determines the longitudinal proton structure function at a rescaled value of  $x \rightarrow \xi_L x$ . The rescaling factor  $\xi_L$  in (2.8) has the preferred value of  $\xi_L \cong 0.40$  [19].

Solving (2.8) for  $G(x, Q^2)$ , allows one to deduce the gluon distribution from measurements of the longitudinal structure function,

$$\begin{aligned} \alpha_s(Q^2) G(x, Q^2) &= \frac{3\pi}{\sum Q_q^2} F_L(\xi_L x, Q^2) \\ &= \frac{3\pi}{\sum Q_q^2} \frac{R}{1+R} F_2(\xi_L x, Q^2), \end{aligned} \quad (2.9)$$

where in the second step, the longitudinal structure function was replaced by the proton structure function  $F_2(\xi_L x, Q^2)$  and the longitudinal-to-transverse ratio,

$$R \equiv \frac{F_L(\xi_L x, Q^2)}{F_T(\xi_L x, Q^2)}. \quad (2.10)$$

A given (analytic) representation of the experimentally measured results for  $F_L(x, Q^2)$ , or for  $F_2(x, Q^2)$  combined with  $R$  is according to (2.10), allows one to deduce an (analytic) expression for the gluon-distribution function according to (2.9).

The accuracy of the approximation of (2.7) by (2.8) for a specific gluon distribution derived from (2.9) for a given structure function  $F_L(\xi_L x, Q^2)$ , may be tested by inserting the result for the gluon distribution deduced from (2.9) into (2.7) (with (2.3)), and subsequently compare the result for  $F_L(x, Q^2)$  thus obtained from (2.7)

with the (experimentally confirmed) structure function that originally entered (2.9) in the determination of the gluon distribution. See Section VI (Table II) for the explicit successful representation of this consistency check for the gluon distribution of the CDP.

### III. THE COLOR-DIPOLE REPRESENTATION.

For a detailed representaion of the CDP, we refer to Refs.[14] and [15]. In a brief summary, the photon interaction (2.5) with the gluon field in the proton at low values of  $x$  is interpreted as fluctuation of the photon into  $q\bar{q}$ -color-dipole states, see (2.6), that interact with the gluon field in the proton via color-gauge-invariant gluon couplings to quark and antiquark states.

In Fig. 1<sup>4</sup>, reproduced from refs. [14, 15], we show the results for the photoabsorption cross section,  $\sigma_{\gamma^*p}(W^2, Q^2)$ , in the CDP. The results are obtained from the explicit analytic expression

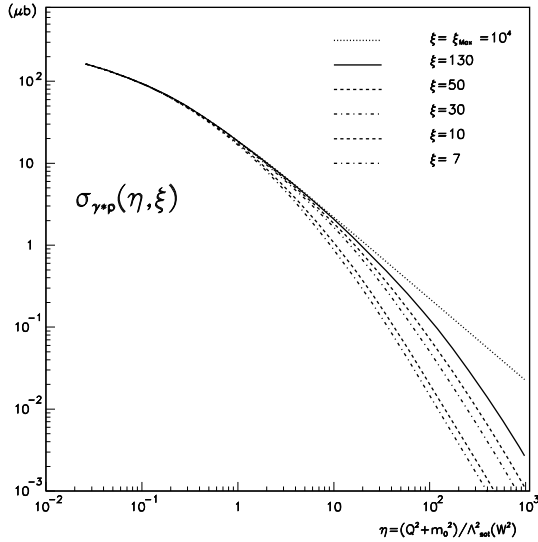


FIG. 1. The theoretical results for the photoabsorption cross section  $\sigma_{\gamma^*p}(\eta(W^2, Q^2), \xi)$  in the CDP as a function of the low- $x$  scaling variable  $\eta(W^2, Q^2) = (Q^2 + m_0^2)/\Lambda_{sat}^2(W^2)$  for different values of the parameter  $\xi$  that determines the (squared) mass range  $M_{q\bar{q}}^2 \leq m_1^2(W^2) = \xi \Lambda_{sat}^2(W^2)$  of the  $\gamma^* \rightarrow q\bar{q}$  fluctuations that are taken into account. The experimental results for  $\sigma_{\gamma^*p}(\eta(W^2, Q^2), \xi)$  lie on the full line corresponding to  $\xi = \xi_0 = 130$ , compare refs. [14, 15].

<sup>4</sup> The photoabsorption cross section (3.1) and (3.2) in good approximation is determined by  $\eta(W^2, Q^2)$ , i.e.  $\sigma_{\gamma^*p}(W^2, Q^2) \cong \sigma_{\rho^*p}(\eta(W^2, Q^2))$  except for a weak (logarithmic)  $W$ -dependence due to  $\sigma^{(\infty)}(W^2)$  in (3.1) or  $\sigma_{\gamma p}(W^2)$  in (3.2). The parameter  $\xi$  (not to be confused with  $\xi_L$ ) is fixed at  $\xi = \xi_0 = 130$ , and for the range of  $\eta(W^2, Q^2)$  of relevance for the present paper, one may put  $\xi \rightarrow \infty$ .

for  $\sigma_{\gamma^*p}(W^2, Q^2)$ ,

$$\begin{aligned} \sigma_{\gamma^*p}(W^2, Q^2) &= \sigma_{\gamma_L^*p}(W^2, Q^2) + \sigma_{\gamma_T^*p}(W^2, Q^2) \\ &= \frac{\alpha R_{e^+e^-}}{3\pi} \sigma^{(\infty)}(W^2) \\ &\quad \times \left( I_T^{(1)}\left(\frac{\eta}{\rho}, \frac{\mu}{\rho}\right) G_T(u) \right. \\ &\quad \left. + I_L^{(1)}(\eta, \mu) G_L(u) \right), \end{aligned} \quad (3.1)$$

derived from an ansatz [13–15] for the  $W$ -dependent dipole cross section that essentially, via the structure of the coupling of the quark-antiquark state to two gluons, represents the color-gauge-invariant interaction of the  $q\bar{q}$  dipole with the gluon-field in the nucleon. In (3.1),  $R_{e^+e^-} = 3 \sum_q Q_q^2$ , where  $q$  runs over the active quark flavors, and  $Q_q$  denotes the quark charge. The smooth transition to  $Q^2 = 0$  photoproduction in (3.1) allows one [15] to replace (see (2.37) in ref. [15])  $\sigma^{(\infty)}(W^2)$ , which stems from the normalization of the  $q\bar{q}$ -dipole-proton cross section<sup>5</sup>, by the photoproduction cross section, and (3.1) becomes

$$\begin{aligned} \sigma_{\gamma^*p}(W^2, Q^2) &= \frac{\sigma_{\gamma p}(W^2)}{\lim_{\eta \rightarrow \mu(W^2)} I_T^{(1)}\left(\frac{\eta}{\rho}, \frac{\mu(W^2)}{\rho}\right) G_T(u)} \\ &\quad \times \left( I_T^{(1)}\left(\frac{\eta}{\rho}, \frac{\mu}{\rho}\right) G_T(u) + I_L^{(1)}(\eta, \mu) G_L(u) \right). \end{aligned} \quad (3.2)$$

We note that  $I_L^{(1)}(\eta, \mu)$  vanishes in the photoproduction  $Q^2 = 0$  limit of  $\eta(W^2, Q^2 = 0) = m_0^2/\Lambda_{sat}^2(W^2) \equiv \mu(W^2)$ , and  $G_T(u \equiv \frac{\xi}{\eta}) \simeq 1$ , and for later reference we also note

$$\lim_{\eta \rightarrow \mu(W^2)} I_T^{(1)}\left(\frac{\eta}{\rho}, \frac{\mu(W^2)}{\rho}\right) = \ln \frac{\rho}{\mu(W^2)}. \quad (3.3)$$

For the general explicit analytic expressions for the functions  $I_T^{(1)}\left(\frac{\eta}{\rho}, \frac{\mu(W^2)}{\rho}\right)$  and  $I_L^{(1)}(\eta, \mu)$  we refer to Appendix

A. The functions  $G_T\left(u \equiv \frac{\xi}{\eta}\right)$  and  $G_L\left(u \equiv \frac{\xi}{\eta}\right)$  are given by

$$G_T(u) = \frac{2u^3 + 3u^2 + 3u}{2(1+u)^3} \simeq \begin{cases} \frac{3}{2} \frac{\xi}{\eta} & , \quad (\eta \gg \xi), \\ 1 - \frac{3}{2} \frac{\eta}{\xi} & , \quad (\eta \ll \xi), \end{cases} \quad (3.4)$$

and

$$G_L(u) = \frac{2u^3 + 6u^2}{2(1+u)^3} \simeq \begin{cases} 3 \left(\frac{\xi}{\eta}\right)^2 & , \quad (\eta \gg \xi), \\ 1 - 3 \left(\frac{\eta}{\xi}\right)^2 & , \quad (\eta \ll \xi), \end{cases} \quad (3.5)$$

<sup>5</sup> Note that the photon fluctuates [13,16] into on-mean-shell massive  $q\bar{q}$  states (see e.g. Ref.[18] for an explicit proof of this point) implying a dipole-proton cross section that depends on  $W^2$  (besides the transverse dipole size) and not on  $x$ , a dependence on  $x$  nevertheless being adopted frequently without justification.

where  $u \equiv \xi/\eta$ , and the constant parameter  $\xi$  restricts the masses of the contributing mass  $q\bar{q}$  states via

$$M_{q\bar{q}}^2 \leq m_1^2(W^2) = \xi \Lambda_{sat}^2(W^2). \quad (3.6)$$

The numerical results for the photoabsorption cross section in Fig. 1 are obtained by numerical evaluation of (3.2) upon insertion of a  $(\ln W^2)^2$  fit to the experimental results for the photoproduction cross section  $\sigma_{\gamma p}(W^2)$  from the Particle Data Group [21]. The results in Fig. 1 were obtained for  $W = 275$  GeV from

$$\begin{aligned} \sigma_{\gamma p}(W^2) = & 0.003056 \left( 34.71 + \frac{0.3894\pi}{M^2} \ln^2 \frac{W^2}{M_p^2 + M^2} \right) \\ & + 0.0128 \left( \frac{(M_p + M)^2}{W^2} \right)^{0.462}. \end{aligned} \quad (3.7)$$

In (3.7),  $M_p$  denotes the proton mass,  $M = 2.15$  GeV and  $\sigma_{\gamma p}(W^2)$  is given in units of millibarn.

Before going into more detail, we note that the full curve in Fig. 1, which for the parameter  $\xi$  corresponds to the choice of  $\xi = \xi_0 = 130$ , provides a representation of the full set of experimental data on  $\sigma_{\gamma^* p}(W^2, Q^2)$  at low  $x \cong Q^2/W^2$ , compare Fig. 8 in ref. [14].

In (3.1) and (3.2), the low- $x$  scaling variable  $\eta(W^2, Q^2)$  is given [13] by

$$\eta \equiv \eta(W^2, Q^2) = \frac{Q^2 + m_0^2}{\Lambda_{sat}^2(W^2)}, \quad (3.8)$$

with

$$\mu \equiv \mu(W^2) = \eta(W^2, Q^2 = 0) = \frac{m_0^2}{\Lambda_{sat}^2(W^2)}, \quad (3.9)$$

the "saturation scale"<sup>6</sup>,  $\Lambda_{sat}^2(W^2)$ , being parametrized by

$$\Lambda_{sat}^2(W^2) = C_1 \left( \frac{W^2}{1 \text{ GeV}^2} \right)^{C_2}, \quad (3.10)$$

and numerically the results in Fig.1 are based on

$$\begin{aligned} m_0^2 &= 0.15 \text{ GeV}^2, \\ C_1 &= 0.31 \text{ GeV}^2; \quad C_2 = 0.27. \end{aligned} \quad (3.11)$$

The parameter  $\rho = \text{const}$  in (3.1) and (3.2) is related to the longitudinal-to-transverse ratio  $R(W^2, Q^2)$  of the photoabsorption cross section, and approximately we have  $R(W^2, Q^2) \simeq 1/2\rho$  for  $\eta(W^2, Q^2) \gg \mu(W^2)$ , while  $R(W^2, Q^2) = 0$  for  $Q^2 = 0$ . The total cross section  $\sigma_{\gamma^* p}(W^2, Q^2)$  is fairly insensitive to the value of  $\rho$  for realistic values of  $\rho$  around  $\rho \cong 1$ , and the evaluation presented in Fig. 1 is based on  $\rho = \frac{4}{3}$ .

In terms of the photoabsorption cross sections  $\sigma_{\gamma_{L,T}^* p}(W^2, Q^2)$ , in (3.1) and (3.2), the proton structure functions, relevant for the extraction of the gluon-density distribution, see (2.9), are given by

$$F_{L,T}(W^2, Q^2) = \frac{Q^2}{4\pi^2\alpha} \sigma_{\gamma_{L,T}^* p}(W^2, Q^2) \quad (3.12)$$

and

$$\begin{aligned} F_2(W^2, Q^2) &= \frac{Q^2}{4\pi^2\alpha} \sigma_{\gamma^* p}(W^2, Q^2) \\ &= \frac{Q^2}{4\pi^2\alpha} (\sigma_{\gamma_T^* p}(W^2, Q^2) + \sigma_{\gamma_L^* p}(W^2, Q^2)). \end{aligned} \quad (3.13)$$

Upon introducing the longitudinal-to-transverse ratio  $R(W^2, Q^2)$  from (2.10), the longitudinal structure function becomes

$$F_L(W^2, Q^2) = \frac{R}{1+R} F_2(W^2, Q^2). \quad (3.14)$$

Explicitly, according to (3.2), we have

$$R(W^2, Q^2) = \frac{I_L^{(1)}(\eta, \mu) G_L(u)}{I_T^{(1)}\left(\frac{\eta}{\rho}, \frac{\mu}{\rho}\right) G_T(u)}. \quad (3.15)$$

For  $Q^2 = 0$ , as a consequence of electromagnetic gauge invariance,

$$R(W^2, Q^2 = 0) = 0, \quad (3.16)$$

while for  $\eta(W^2, Q^2)$ , restricted by the interval of  $1 \ll \eta(W^2, Q^2) \ll \xi = \xi_0 = 130$  that will be of relevance subsequently, we have

$$R(W^2, Q^2) \approx \frac{1}{2\rho}, \quad (3.17)$$

with  $\rho = \text{const}$  in the vicinity of  $\rho \cong 1$ , and, accordingly, (3.14) becomes

$$\begin{aligned} F_L(W^2, Q^2) &= \frac{1}{2\rho + 1} F_2(W^2, Q^2), \\ (1 \ll \eta(W^2, Q^2) \ll \xi_0). \end{aligned} \quad (3.18)$$

While (3.18) holds strictly for sufficiently large  $Q^2$ , even for low values of  $Q^2 \gtrsim 1 \text{ GeV}^2$  it may be used as an approximation of (3.14). The accuracy of (3.18) as approximation for low  $Q^2$  is seen by comparing the results in Fig.3 and Fig.4 in Section V below.

For large  $Q^2$ , specifically for  $10 \text{ GeV}^2 \lesssim Q^2 \lesssim 100 \text{ GeV}^2$  the range of  $Q^2$  of particular relevance in connection with pQCD, the experimental data on the proton structure function  $F_2(W^2, Q^2)$  in (3.13) depend on the single variable  $W^2$ , compare Fig. 2 quoted from ref. [14].

A simple two-parameter eye-ball fit to the experimental data in Fig. 2 yields [14]

$$F_2(W^2) = f_2 \left( \frac{W^2}{1 \text{ GeV}^2} \right)^{C_2}, \quad (3.19)$$

<sup>6</sup> The value of  $\Lambda_{sat}^2(W^2)$  via  $\eta(W^2, Q^2) \cong 5$  determines the transition from color transparency of  $\eta(W^2, Q^2) \gtrsim 5$  to hadronlike saturation of  $\eta \lesssim 5$ .

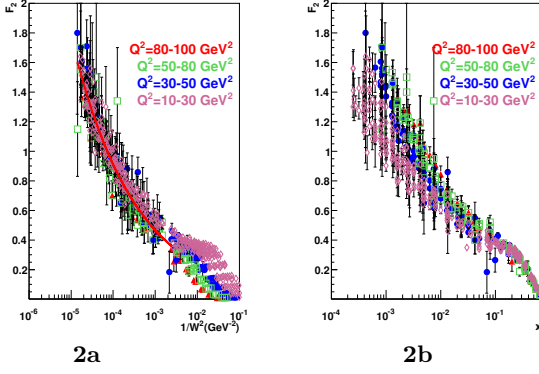


FIG. 2. In Fig.2a we show the experimental data for  $F_2(x \cong Q^2/W^2, Q^2)$  as a function of  $1/W^2$ , and in Fig.2b, for comparison, as a function of  $x$ . The theoretical prediction based on (3.19) with (3.20) is also shown in Fig.2a.

where <sup>7</sup>

$$f_2 = 0.063, \quad C_2 = 0.29. \quad (3.20)$$

The fit result is understood as a consequence of the CDP in the large- $\eta(W^2, Q^2)$  approximation. The structure function  $F_2(W^2, Q^2)$  for  $Q^2 \gg \Lambda_{sat}^2(W^2)$  according to (3.13) upon substitution of (3.1) takes the simple form

$$F_2(W^2, Q^2) = \frac{R_{e^+e^-}\sigma^{(\infty)}(W^2)}{24\pi^3} \frac{1+2\rho}{3} \Lambda_{sat}^2(W^2) \times \left(1 + 0\left(\frac{1}{\eta}\right)\right). \quad (3.21)$$

Upon specifying  $\Lambda_{sat}^2(W^2) = C_1 \left(\frac{W^2}{1\text{GeV}^2}\right)^{C_2}$  according to (3.10), the structure function (3.21) can directly be compared with (3.19),

$$F_2(W^2, Q^2) = \frac{R_{e^+e^-}\sigma^{(\infty)}(W^2)}{24\pi^3} \frac{1+2\rho}{3} C_1 \left(\frac{W^2}{1\text{GeV}^2}\right)^{C_2} \times \left(1 + 0\left(\frac{1}{\eta}\right)\right) \equiv \hat{f}_2(W^2) \left(\frac{W^2}{1\text{GeV}^2}\right)^{C_2} \left(1 + 0\left(\frac{1}{\eta}\right)\right). \quad (3.22)$$

The product  $R_{e^+e^-}\sigma^{(\infty)}(W^2)$  is determined by the photoproduction cross section (3.7) according to

$$R_{e^+e^-}\sigma^{(\infty)}(W^2) = \frac{3\pi}{\alpha} \frac{\sigma_{\gamma p}(W^2)}{\ln \frac{\rho \Lambda_{sat}^2(W)}{m_0^2}}, \quad (3.23)$$

compare to (3.1) to (3.3).

<sup>7</sup> The value of the exponent  $C_2 = 0.29$  is consistent [20] with the independent fit to the DIS experimental data based on the hard-Pomeron conjecture leading to the exponent  $C_0 \cong 0.30 \pm 0.1$ .

For definiteness, in Table 1, we explicitly present the input for the evaluation of  $F_2$  according to (3.22) that leads to

$$\hat{f}_2(W^2) = \begin{cases} 0.067 & , \text{ for } W^2 = 10^4 \text{ GeV}^2, \\ 0.068 & , \text{ for } W^2 = 10^5 \text{ GeV}^2. \end{cases} \quad (3.24)$$

TABLE I. The evaluation of  $\hat{f}_2(W^2)$  defined by (3.22). The parameters  $\rho$  and  $m_0^2$  in (3.22) and (3.23) are given by  $\rho = 4/3$  and  $m_0^2 = 0.15 \text{ GeV}^2$ .

$W^2$ [GeV <sup>2</sup> ]	$10^4$	$10^5$
$\sigma_{\gamma p}$ [mb]	0.146	0.175
$\Lambda_{sat}^2(W^2) = C_1 \left(\frac{W^2}{1\text{GeV}^2}\right)^{C_2}$		
$C_1 = 0.31 \text{ GeV}^2$ , $C_2 = 0.29$	4.48	8.74
$R_{e^+e^-}\sigma^{(\infty)}(W^2)$ [mb]	50.9	51.9
$\hat{f}_2(W^2)$	0.067	0.068

These values of  $\hat{f}_2(W^2)$  are approximately 6 % to 7 % larger than the values from the eye-ball fit (3.19) in (3.20). The structure function  $F_2(W^2, Q^2)$  is given by

$$F_2 \cong \begin{cases} 0.96 & , \text{ for } W^2 = 10^4 \text{ GeV}^2, \\ 1.91 & , \text{ for } W^2 = 10^5 \text{ GeV}^2. \end{cases} \quad (3.25)$$

For the determination of the gluon distribution according to (2.9), the structure functions in (3.12) and (3.13) have to be evaluated at a rescaled or shifted value of  $x \rightarrow \xi_L x$ , corresponding to a shift of  $W^2 \rightarrow \xi_L^{-1} W^2$ . In terms of the low- $x$  scaling variable  $\eta(W^2, Q^2)$ , the shift becomes

$$\eta(W^2, Q^2) = \frac{Q^2 + m_0^2}{\Lambda_{sat}^2(W^2)} \rightarrow \frac{Q^2 + m_0^2}{\Lambda_{sat}^2(\xi_L^{-1} W^2)}. \quad (3.26)$$

For

$$\Lambda_{sat}^2(W^2) = C_1 \left(\frac{W^2}{1 \text{ GeV}^2}\right)^{C_2}, \quad (3.27)$$

to be employed subsequently, the shift becomes

$$\eta(W^2, Q^2) \rightarrow \xi_L^{C_2} \eta(W^2, Q^2). \quad (3.28)$$

The photoabsorption cross section (3.2) essentially only depends on  $\eta(W^2, Q)$ ,

$$\sigma_{\gamma_{L,T}^* p}(W^2, Q^2) \cong \sigma_{\gamma_{L,T}^* p}(\eta(W^2, Q^2)), \quad (3.29)$$

since the  $Q^2 = 0$  photoproduction factor in (3.2) depends only weakly on  $W^2$ . The rescaling shift (3.28) applied to the cross section (3.2), accordingly, amounts to

$$\sigma_{\gamma_{L,T}^* p}(\eta(W^2, Q^2)) \rightarrow \sigma_{\gamma_{L,T}^* p}(\xi_L^{C_2} \eta(W^2, Q^2)). \quad (3.30)$$

Numerically, for  $C_2 = 0.29$  and  $\xi_L = 0.4$ , we have

$$\xi_L^{C_2} \eta = 0.4^{0.29} \eta \cong 0.77 \eta(W^2, Q^2). \quad (3.31)$$

Explicitly, the gluon distribution (2.9) becomes

$$\alpha_s(Q^2)G(x, Q^2) = \frac{3\pi}{\sum_q Q_q^2} \frac{Q^2}{4\pi^2\alpha} \sigma_{\gamma_L^* p} \left( \xi_L^{C_2} \eta(W^2, Q^2) \right). \quad (3.32)$$

We note that (3.32) provides the connection between the gluon distribution (the basic quantity of the pQCD-improved parton model) and the dipole cross section (the basic quantity of the CDP), since  $\sigma_{\gamma_L^* p}$  in (3.32) may be replaced by the dipole cross section  $\sigma_{(q\bar{q})p}(r_\perp, z(1-z), W^2 = \frac{Q^2}{x})$ , according to

$$\sigma_{\gamma_L^* p}(W^2 = \frac{Q^2}{x}, Q^2) = \int dz \int d^2 r_\perp |\Psi_L(r_\perp, z(1-z), Q^2)|^2 \times \sigma_{(q\bar{q})p}(r_\perp, z(1-z), W^2 = \frac{Q^2}{x}). \quad (3.33)$$

The empirically verified low- $x$  scaling of the photoabsorption cross section in the variable  $\eta(W^2, Q^2)$  translates from the photoabsorption cross section to the gluon distribution divided by  $Q^2$ . For sufficiently large  $Q^2$ , with  $\sigma_{\gamma_L^* p} \propto \Lambda_{sat}^2(W^2)/Q^2$  [15], according to (3.32) we obtain the asymptotic behavior of

$$\alpha_s(Q^2)G(x, Q^2) \propto \Lambda_{sat}^2(W^2). \quad (3.34)$$

The quantity  $\Lambda_{sat}^2(W^2)$ , also known as saturation scale, determines the gluon distribution function in the pQCD large- $Q^2$  limit.

The arguments in Section II and the present Section III may be summarized as follows: In the CDP, at leading order of pQCD, DIS at low  $x$  is (successfully) described as interaction of the photon with the  $q\bar{q}$  sea according to (2.6). This implies that the pQCD equation (2.1) for the longitudinal proton structure function can be approximated by the gluon contribution, see (2.7), and, finally the gluon distribution can be determined by (2.9). On the right-hand side, the proton structure function from the CDP has to be substituted.

Independently from the CDP, the approximation of (2.1) by (2.9) as leading term at large  $Q^2$  was justified [19] by evaluating suitable models for the gluon distribution.

Note that the pQCD equation (2.9) for its validity requires sufficiently large values of  $Q^2$ . Since the CDP description by the proton structure functions to substituted into (2.9) includes the low- $Q^2$  limit, equation (2.9) contains a smooth extrapolation of the gluon density to low values of  $Q^2$ .

#### IV. THE FROISSART-BOUNDED REPRESENTATION OF $F_2(x, Q)$ .

A very accurate fit to the measured proton structure function of DIS, due to Block et al. [22], is pro-

vided by a representation of the DIS data saturating the  $(\log W^2)^2$  bound derived from general-field-theory principles by Froissart [23]. Even though the determination of the gluon distribution (2.9) contains the CDP representation for the proton structure function, one may expect that different precise fits to the DIS data will at least approximately lead to the same results for the gluon distribution. In this spirit, we shall employ the Froissart-bounded representation in addition to the CDP representation for the proton structure function.

The results from DIS at low  $x \leq 0.1$  and for a large range of  $Q^2$  from  $0.15 \text{ GeV}^2 \leq Q^2 \leq 3000 \text{ GeV}^2$  are represented by the structure function [22]

$$F_2(x, Q^2) = D(Q^2)(1-x)^n [C(Q^2) + A(Q^2) \ln \left( \frac{1}{x} \frac{Q^2}{Q^2 + \mu^2} \right) + B(Q^2) \ln^2 \left( \frac{1}{x} \frac{Q^2}{Q^2 + \mu^2} \right)]. \quad (4.1)$$

The power  $n$  and the scale  $\mu^2$  are given by  $n = 11.49 \pm 0.99$  and  $\mu^2 = 2.82 \pm 0.290 \text{ GeV}^2$ . The logarithmic dependence on  $Q^2$  of the functions  $A(Q^2), B(Q^2), C(Q^2)$  and  $D(Q^2)$  is given in Appendix B and Table B1 reproducing Table II from ref. [22].

In distinction from the CDP, the Froissart-bounded fit does not explicitly provide a representation of the longitudinal-to-transverse ratio  $R$ . When deducing the gluon distribution function, the value of  $R$  from the CDP will have to be adopted.

#### V. THE RESULTS FOR THE GLUON DISTRIBUTION FUNCTION.

We turn to the explicit results for the gluon distribution which follow from the evaluation of (2.9) upon substitution of the representation of the DIS experimental results in the CDP and the Froissart-bounded representation, as given in Sections III and IV, respectively.

Substitution into (2.9) of the CDP results (3.12) with (3.2) for  $F_L(W^2, Q^2)$  yields

$$\alpha_s(Q^2)G(x, Q^2) = \frac{3\pi}{\sum_q Q_q^2} F_L(\xi_L x, Q^2) = \frac{9Q^2}{4\pi\alpha R_{e^+e^-}} \times \left( \frac{\sigma_{\gamma p}(W^2)}{\left( \ln \frac{E}{\mu} \right) G_T \left( \frac{\xi}{\eta} \right)} I_L^{(1)}(\eta, \mu) G_L \left( \frac{\xi}{\eta} \right) \right) \Big|_{W^2 \rightarrow \xi_L^{-1} W^2} \quad (5.1)$$

The variables  $\eta = \eta(W^2, Q^2)$  and  $\mu(W^2)$  are given by (see (3.8), (3.9)),

$$\eta(W^2, Q^2) = \frac{Q^2 + m_0^2}{\Lambda_{sat}^2(W^2)}, \quad \mu(W^2) = \frac{m_0^2}{\Lambda_{sat}^2(W^2)}, \quad (5.2)$$

where

$$\Lambda_{sat}^2(W^2) = C_1(W^2)^{C_2} = 0.31 \left( \frac{W^2}{1\text{GeV}^2} \right)^{0.29} \text{GeV}^2, \quad (5.3)$$

with  $C_2 = 0.29$  from (3.20) and

$$m_0^2 = 0.15 \text{ GeV}^2. \quad (5.4)$$

For the assumed number of four flavors,

$$R_{e^+e^-} \equiv 3 \sum_q Q_q^2 = \frac{10}{3}. \quad (5.5)$$

The parameter  $\rho$ , denoting the size enhancement of transversely relative to longitudinally polarized  $q\bar{q}$  fluctuations, is given by [24]

$$\rho = \frac{4}{3}. \quad (5.6)$$

The parameter  $\xi$  that stands for the upper limit,  $\xi \Lambda_{sat}^2(W^2)$ , of masses of  $q\bar{q}$  fluctuations actively contributing, is given by  $\xi = 130$ . At the relevant (low) values of  $\eta(W^2, Q^2)$ , the limit of  $\xi \rightarrow \infty$  and  $G_T\left(\frac{\xi}{\eta}\right) = G_L\left(\frac{\xi}{\eta}\right) = 1$  (see (3.4) and (3.5)) may be taken without loss of generality, compare Fig. 1. The  $\log(W^2)$  fit to the photoproduction experimental results is given by (3.7), and, finally, the shift factor  $\xi_L$  according to (2.8) is given by

$$\xi_L = 0.4. \quad (5.7)$$

The essential effect of the shift  $W^2 \rightarrow \xi_L^{-1} W^2$ , in (5.1) amounts to

$$\eta(W^2, Q^2) \rightarrow \xi_L^{C_2} \eta(W^2, Q^2), \quad (5.8)$$

compare (3.30), the  $Q^2 = 0$  photoproduction term in (5.1), including its normalization by the denominator in (5.1), being hardly affected due to its weak dependence on  $W^2$ .

According to (2.9), the gluon distribution may equivalently be expressed in terms of the structure function  $F_2(\xi_L x, Q^2)$  instead of  $F_L(\xi_L x, Q^2)$ , together with the longitudinal-to-transverse ratio  $R$ . For sufficiently large  $Q^2$ , according to (2.9) and (3.18), with  $R = 1/2\rho$ ,

$$\alpha_s(Q^2)G(x, Q^2) = \frac{9\pi}{R_{e^+e^-}} \frac{1}{2\rho + 1} F_2(\xi_L x, Q^2). \quad (5.9)$$

As noted in connection with (3.18), representation (5.9), even at small  $Q^2$  may be used as an approximation of the gluon distribution.

For  $Q^2$  sufficiently large, specifically for  $20 \text{ GeV}^2 \lesssim Q^2 \lesssim 100 \text{ GeV}^2$ , the large- $Q^2$  limit of (5.1) given by

(3.19) becomes relevant. It implies the simple large- $Q^2$  representation of

$$\begin{aligned} \alpha_s(Q^2)G(x, Q^2) &= \frac{9\pi}{R_{e^+e^-}} \frac{1}{(2\rho + 1)} F_2(\xi_L x, Q^2) \\ &= \frac{9\pi}{R_{e^+e^-}} \frac{1}{(2\rho + 1)} f_2 \xi_L^{-0.29} \left( \frac{W^2}{1\text{GeV}^2} \right)^{C_2=0.29}, \end{aligned} \quad (5.10)$$

where  $f_2 = 0.063$ , and  $\rho = \frac{4}{3}$ .

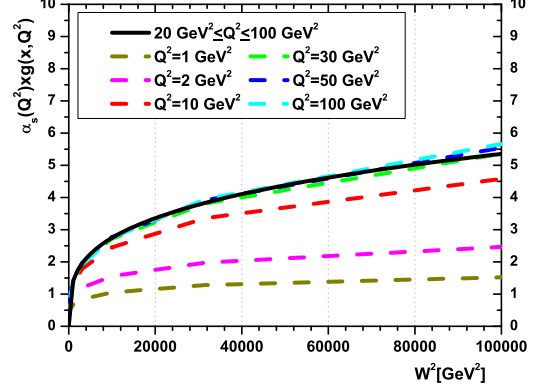


FIG. 3. The gluon distribution  $\alpha_s(Q^2)xg(x, Q^2) \equiv \alpha_s(Q^2)G(x, Q^2)$  of the CDP, compare (5.1), as a function of  $W^2$  for various values of  $Q^2$ . The solid line shows the asymptotic limit (5.10) that is reached at  $Q^2 \gtrsim 30 \text{ GeV}^2$ .

In Fig. 3, we show the gluon distribution (2.9) deduced from  $F_L(W^2, Q^2)$  according to (5.1) as a function of  $W^2$  for various values of  $Q^2$ , where  $1 \text{ GeV}^2 \leq Q^2 \leq 100 \text{ GeV}^2$ . The results in Fig. 3, for  $Q^2$  sufficiently above  $Q^2 \cong 10 \text{ GeV}^2$ , indeed converge towards the asymptotic representation (5.10).

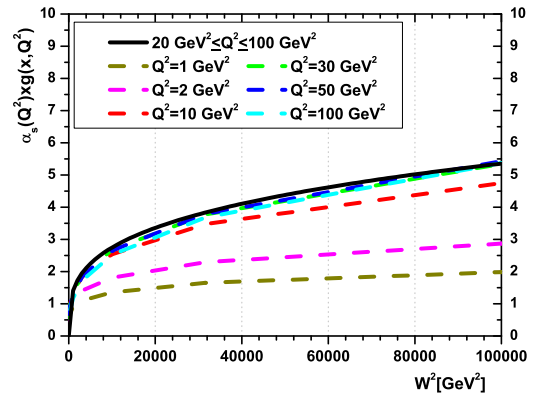


FIG. 4. As Fig. 3, but based on (5.9), employing  $R = \text{const} = 1/2\rho = 3/8$ . Compare text for details.

The results in Fig. 4, for low  $Q^2$ ,  $1\text{GeV}^2 \leq Q^2 \leq 10\text{GeV}^2$ , compared with the results in Fig. 3, show the enhanced gluon distribution resulting from employing the large- $Q^2$  approximation (5.9). For sufficiently large  $Q^2$ , the results in Fig. 4, based on  $F_2(\xi_L x, Q^2)$  according to (3.18) and (5.9), coincide with the ones in Fig. 3 based on  $F_L(\xi_L x, Q^2)$  according to (5.1).

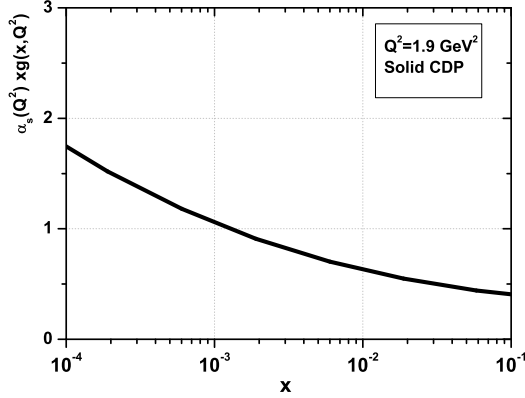


FIG. 5. The gluon-distribution function  $\alpha_s(Q^2)xg(x, Q^2)$  of the CDP as a function of  $x \cong Q^2/W^2$  at the (low) value of  $Q^2 = 1.9\text{ GeV}^2$ , the scale frequently used as input scale [6].

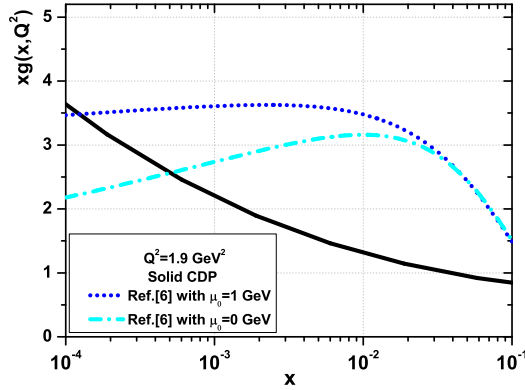


FIG. 6. As Fig. 5, but for  $xg(x, Q^2)$  instead of  $\alpha_s(Q^2)xg(x, Q^2)$ . The CDP results are compared with the results from ref.[6].

For Figs. 5 and 6, the energy variable,  $W$ , of the CDP is replaced by  $x \cong Q^2/W^2$ . The increase of  $x$  for  $Q^2 = 1.9\text{ GeV}^2$  in the range of  $10^{-4} \leq x \leq 10^{-1}$  corresponds to an increase of  $\eta(W^2, Q^2 = 1.9\text{ GeV}^2)$  according to  $0.35 \leq \eta \leq 2.6$ , with  $W^2$  decreasing according to  $1.9 \times 10^4 \text{ GeV}^2 \geq W^2 \geq 19 \text{ GeV}^2$ . Taking into account the proportionality of the gluon distribution to the longitudi-

nal photoabsorption cross section (3.32), and consulting the results in Fig. 1, we expect a (hadronlike) increase of the gluon distribution by a factor of approximately about 3.5 with decreasing  $x$  in the interval  $10^{-1} \geq x \geq 10^{-4}$ . This factor of 3.5 for  $x = 10^{-4}$  is seen in Figure 5.

Multiplication of the results in Fig. 5 by  $\alpha_s(Q^2 = 1.9\text{ GeV}^2)^{-1} = 0.480^{-1} = 2.083$  yields the results for  $xg(x, Q^2) \equiv G(x, Q^2)$  that are shown in Fig. 6<sup>8</sup>

In Fig. 6, we compare with the results obtained in ref. [6] upon introducing absorptive corrections to the measured proton structure functions, and a modification of  $\alpha_s(Q^2)$  by  $\alpha_s(Q^2 + \mu_0^2)$ . The gluon distributions from ref. [6] in Fig. 6 are given by [6]

$$\begin{aligned} xg(x) &= 5.63x^{0.103}(1-x)^{10.261} \text{ for } \mu_0 = 0\text{ GeV}, \\ xg(x) &= 4.21x^{0.021}(1-x)^{9.427} \text{ for } \mu_0 = 1\text{ GeV}. \end{aligned} \quad (5.11)$$

As seen in Fig. 6, the results from ref. [6] are drastically different from ours. The results obtained by exploiting the smooth low- $Q^2$  transition for  $F_L(x, Q^2)$  of the CDP by substitution into the pQCD-improved parton model do not support the modifications of evolution suggested and applied to DIS in Ref.[6]. For further discussions on the consequences of our approach of incorporating the CDP representation for  $F_L(x, Q^2)$  into pQCD, see sections VI and VII.

For completeness, in Fig.7, we show the CDP gluon distribution for  $Q^2$  between  $Q^2 = 2\text{ GeV}^2$  and  $Q^2 = 100\text{ GeV}^2$ .

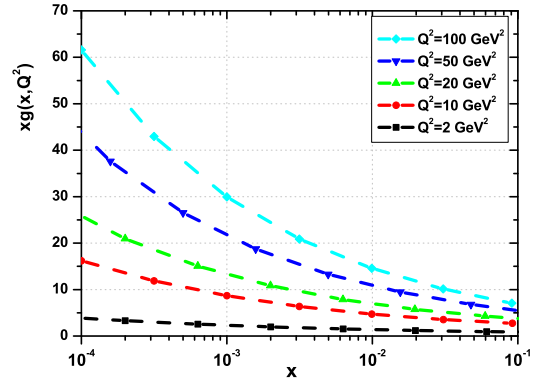


FIG. 7. The CDP gluon distribution  $xg(x, Q^2)$  in a wide range of  $Q^2$  values,  $2\text{ GeV}^2 \leq Q^2 \leq 100\text{ GeV}^2$

The analysis of the gluon distribution function that led to the results in Figs. 3 to 7 is based on the representation of the proton structure functions in the CDP. We

<sup>8</sup> The value of  $\alpha_s(Q^2 = 1.9\text{ GeV}^2) = 0.480$  is obtained for  $\Lambda_{QCD} = 437\text{ MeV}$  corresponding to  $\alpha_s(M_Z^2) = 0.118$ .



expect that other precise and theoretically well-founded representations of the measured structure functions will lead to (at least approximately) identical results for the gluon distribution. Explicitly this equivalence is tested by the example of employing the fit to the proton structure function in the Froissart-bounded representation<sup>9</sup> from ref. [22], described in Section IV.

Since the theoretical representation in this approach does not isolate the longitudinal structure function, the gluon distribution must be deduced from  $F_2(\xi_L x, Q^2)$  with  $\rho = \frac{4}{3}$  in (5.9).

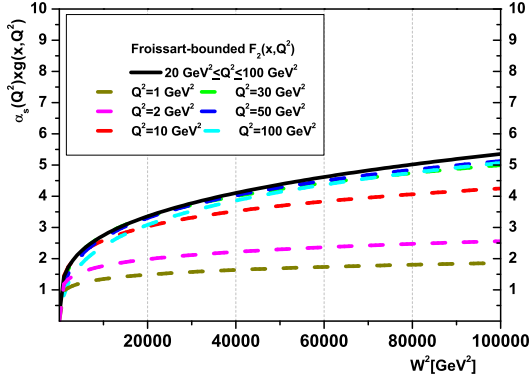


FIG. 8. The gluon distribution  $\alpha_s(Q^2)xg(x, Q^2)$  deduced from the Froissart-bounded representation of the proton structure function  $F_2(x, Q^2)$  given in ref. [22]

The results in Fig. 8 for large  $Q^2$ , asymptotically, agree with the CDP result. For  $Q^2 \lesssim 10 \text{ GeV}^2$ , there are acceptable deviations, seen upon comparing the results in Fig. 8 with the ones in Figs. 3 and 4.

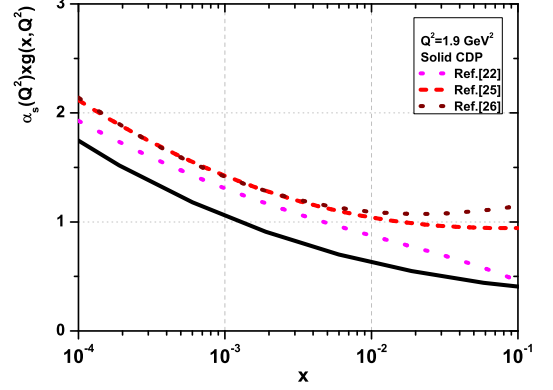


FIG. 9. The gluon-distribution function  $\alpha_s(Q^2)xg(x, Q^2)$  as a function of  $x \cong Q^2/W^2$  at  $Q^2 = 1.9 \text{ GeV}^2$  from the CDP, and from Froissart-bounded representations in refs. [22], [25] and [26].

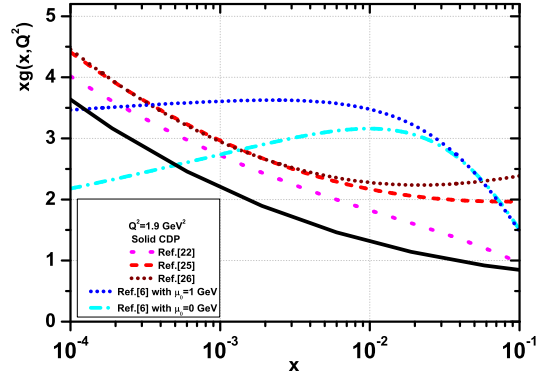


FIG. 10. Same as Fig. 9 except for showing  $xg(x, Q^2)$  instead of  $\alpha_s(Q^2)xg(x, Q^2)$ . The CDP results and the results from the Froissart-bounded representation are compared with the results from ref. [6].

In Figs. 9 and 10, respectively, we present the comparison of the gluon distribution from the Froissart-bounded representation of  $F_2(x, Q^2)$  with the results based on the CDP, and with the results from ref. [6] at  $Q^2 = 1.9 \text{ GeV}^2$  based on pQCD modified by power law corrections and absorptive effects. In addition to the results extracted from the fit to the proton structure function described in Section IV., in Figs. 9 and 10, we have employed [22] two additional somewhat different fits from refs. [25, 26] without entering into a detailed description of these fits.

By comparison of the results on the gluon distribution deduced from the representation of the body of DIS experimental data of the proton structure functions in the CDP, and the Froissart-bounded approach, at

<sup>9</sup> We evaluate the gluon distribution from the pQCD approximation (2.9) as well as (6.5) below, in distinction from the approach in ref. [22] that is based on an exact determination of  $G(x, Q^2)$  [25] upon converting (6.1) below into an inhomogeneous second order differential equation for  $G(x, Q^2)$ .

$Q^2 = 1.9 \text{ GeV}^2$ , we find a consistent behavior as expected.

The shape and the absolute magnitude of the gluon distribution according to Fig.10 is significantly different from results recently presented in ref.[6].

## VI. THE CONSISTENCY OF PQCD AND CDP EVOLUTION AT LARGE $Q^2$

As indicated at the end of section II, we examine the reliability of the approximation (2.8) of replacing the integral over the gluon distribution (2.7) by the rescaling shift  $x \rightarrow \xi_L x$  or  $W^2 \rightarrow \xi_L^{-1} W^2$ , according to (2.8), as employed in the determination of the gluon distribution according to (5.1).

TABLE II. The Table shows the ratio of  $F_L(W^2, Q^2)$  from pQCD according to (2.8) upon substitution of (2.9), to  $F_L(W^2, Q^2)$  from (3.12) with (3.2). Compare text for more detail.

	$W^2 = 10^5$ [GeV <sup>2</sup> ]	$W^2 = 10^4$ [GeV <sup>2</sup> ]	$W^2 = 10^3$ [GeV <sup>2</sup> ]
$Q^2 = 100$ [GeV <sup>2</sup> ]	1.043	1.037	0.981
$Q^2 = 50$ [GeV <sup>2</sup> ]	1.041	1.037	1.012
$Q^2 = 10$ [GeV <sup>2</sup> ]	1.035	1.035	1.030
$Q^2 = 1$ [GeV <sup>2</sup> ]	1.015	1.021	1.026

In Table II, we show the ratio of the structure function  $F_L(W^2, Q^2)$ , thus obtained from (2.8) upon insertion of (2.9) into (2.8), to the CDP structure function  $F_L(W^2, Q^2)$  in (3.12) with (3.2) that was used as input in evaluating the scaling-shift formula (5.1) identical to (2.9). The deviations of this ratio from unity is below 5 %. The determination of the gluon distribution function by replacing the original pQCD result (2.7) by the approximation (2.8) is indeed a reliable one.

The  $Q^2$  dependence of the gluon distribution function according to (5.1) and (5.9) is determined by the  $Q^2$  dependence of the proton structure functions in the CDP.

In the main part of this Section, we examine the consistency of the  $Q^2$  evolution thus obtained for the gluon distribution from the CDP, with the  $Q^2$  dependence predicted from pQCD. To order  $\alpha_s(Q^2)$ , only process (2.5) contributes, and accordingly we can restrict ourselves to investigating the consistency of the  $Q^2$  dependence from the CDP with the  $Q^2$  dependence from the first DGLAP evolution equation [9].

The change of  $F_2(x, Q^2)$  with  $Q^2$ , its evolution at large

$Q^2$ , is given by [9]

$$\frac{\partial}{\partial \ln Q^2} F_2(x, Q^2) = \frac{\alpha_s(Q^2)}{2\pi} \int_x^1 dz P_{qq}(z) F_2\left(\frac{x}{z}, Q^2\right) + \frac{R_{e^+e^-}}{3\pi} \alpha_s(Q^2) \int_0^{1-x} dz P_{qg}(z) G\left(\frac{x}{1-z}, Q^2\right), \quad (6.1)$$

where

$$P_{qq}(z) = \frac{4}{3} \left( \frac{1+x^2}{(1-x)_+} + \frac{3}{2} \delta(1-x) \right), \quad (6.2)$$

and

$$P_{qg}(z) = \frac{1}{2} (z^2 + (1-z)^2). \quad (6.3)$$

According to our basic assumption (2.7), saying that the photon exclusively interacts with  $q\bar{q}$  pairs originating from a gluon,  $g \rightarrow q\bar{q}$  see (2.6), we exclude the first term on the right-hand side in (6.1) to obtain [27]

$$\frac{\partial F_2(x, Q^2)}{\partial \ln Q^2} = \frac{R_{e^+e^-}}{3\pi} \int_0^{1-x} dz P_{qg}(z) G\left(\frac{x}{1-z}, Q^2\right). \quad (6.4)$$

Exploiting the symmetry of  $P_{qg}(z)$  in (6.4) around  $z = 1/2$ , the first derivative of  $G(x/(1-z), Q^2)$  in a Taylor expansion of  $G(x/(1-z), Q^2)$  around  $z = \frac{1}{2}$  yields a vanishing contribution to the integral in (6.4), and approximately [27]

$$\frac{\partial F_2(x, Q^2)}{\partial \ln Q^2} = \frac{R_{e^+e^-}}{9\pi} \alpha_s(Q^2) G\left(\frac{x}{\xi_2}, Q^2\right). \quad (6.5)$$

with  $x/\xi_2 = 2x$ , or  $\xi_2 = 1/2$ . Replacing the gluon distribution in (6.5) by its proportionality (2.9) to the structure function  $F_L$ , (6.5) becomes

$$\frac{\partial F_2(x, Q^2)}{\partial \ln Q^2} = F_L\left(\frac{\xi_L}{\xi_2} x, Q^2\right) = \frac{1}{2\rho+1} F_2\left(\frac{\xi_L}{\xi_2} x, Q^2\right), \quad (6.6)$$

where the second equality is due to (3.18).

So far no specific ansatz for the proton structure function was used. Introducing the large- $Q^2$  power-law of the CDP (3.21) with (3.10),

$$F_2(x, Q^2) \sim (W^2)^{C_2} = \left(\frac{Q^2}{x}\right)^{C_2}, \quad (6.7)$$

from (6.6) we obtain the important constraint

$$C_2 \left(\frac{Q^2}{x}\right)^{C_2} = \frac{1}{2\rho+1} \left(\frac{Q^2}{x}\right)^{C_2} \left(\frac{\xi_2}{\xi_L}\right)^{C_2}, \quad (6.8)$$

or

$$C_2(2\rho+1) \left(\frac{\xi_L}{\xi_2}\right)^{C_2} = 1. \quad (6.9)$$

Expansion of the exponential to first order in  $C_2$  yields the convenient expression for  $C_2$ ,

$$C_2 \cong \frac{1}{2\rho+1} \frac{1}{\left(1 - \frac{1}{2\rho+1} \ln \frac{\xi_2}{\xi_L}\right)}. \quad (6.10)$$

For  $\xi_2/\xi_L = 0.5/0.4 = 1.25$ , with  $\rho = \frac{4}{3}$ , one finds  $C_2 \cong 0.29$  for the exponent  $C_2$  in (6.9).

The prediction of  $C_2 \cong 0.29$  is based on the assumption that the evolution in  $Q^2$  is entirely due to  $q\bar{q}$  pairs originating from gluons  $g \rightarrow q\bar{q}$ , see (6.4) and (6.5). The agreement of the prediction of  $C_2 \cong 0.29$  from (6.9) with the experimentally determined value, given in (3.20), provides empirical evidence for, or confirms the approximation of reducing the complete evolution equation (6.1) to the reduced form (6.5) employed to arrive at (6.9). The incoming photon dominantly interacts with  $q\bar{q}$  pairs originating from the  $g \rightarrow q\bar{q}$  transition, see (2.6).

We conclude: the CDP with the power-law ansatz for  $F_2(x, Q^2) \sim (Q^2/x)^{C_2}$  for large  $Q^2$  fulfills evolution according to (6.4) with  $Q^2$  at large  $Q^2$ , and it implies the empirically successful prediction of  $C_2 \cong 0.29$ .

## VII. EVOLUTION AT LOW $Q^2 \gtrsim 1.9\text{GeV}^2$ .

In considering the validity of the pQCD evolution equation (6.5) for  $F_2(x, Q^2)$ , we so far restricted ourselves to large values of  $Q^2$ , sufficiently large with respect to  $\Lambda_{sat}^2(W^2)$ , effectively,  $Q^2 \gtrsim 10\text{GeV}^2$  to  $20\text{GeV}^2$ . Employing the large- $Q^2$ -representation for  $F_2(x, Q^2) \sim \left(\frac{Q^2}{x}\right)^{C_2}$ , the validity of the evolution equation (6.6) implied the restriction (6.9) that predicts the exponent  $C_2$  in  $\Lambda_{sat}^2(W^2) \sim (W^2)^{C_2}$  in terms of the transverse- $q\bar{q}$ -size parameter  $\rho$ , where  $\rho$  has the preferred value [24] of  $\rho = 4/3$ .

In the present Section, we lift the restriction on the magnitude of  $Q^2$  by allowing for values of  $Q^2$  as low as  $Q^2 \gtrsim 1.9\text{GeV}^2$ , the value frequently adopted [6] when applying pQCD to electron-proton DIS.

The CDP proton structure functions entering (6.6) according to (3.1), (3.2) and (3.12), without restriction to large  $Q^2$  are given by

$$\begin{aligned} F_2(x, Q^2) &\equiv F_2\left(\eta\left(W^2 = \frac{Q^2}{x}, Q^2\right), \mu\left(W^2 = \frac{Q^2}{x}\right)\right) \\ &= \frac{Q^2}{4\pi^2\alpha} \frac{\sigma_{\gamma p}(W^2)}{\ln \frac{\rho}{\mu(W^2)}} \left(I_T^{(1)}\left(\frac{\eta}{\rho}, \frac{\mu}{\rho}\right) G_T(u) + I_L^{(1)}(\eta, \mu) G_L(u)\right), \end{aligned} \quad (7.1)$$

and

$$\begin{aligned} F_L(x, Q^2) &\equiv F_L\left(\eta\left(W^2 = \frac{Q^2}{x}, Q^2\right), \mu\left(W^2 = \frac{Q^2}{x}\right)\right) \\ &= \frac{Q^2}{4\pi^2\alpha} \frac{\sigma_{\gamma p}(W^2)}{\ln \frac{\rho}{\mu(W^2)}} I_L^{(1)} G_L(u). \end{aligned} \quad (7.2)$$

The fit to the experimental data of  $\sigma_{\gamma p}(W^2)$  is given by (3.7). For the explicit expressions for  $I_T^{(1)}$  and  $I_L^{(1)}$  in (7.1) and (7.2), we refer to Appendix A. In the present context we can restrict ourselves to the range of  $\eta \ll \xi = 130$ , and accordingly  $G_{L,T}(u) = 1$  in (7.1) and (7.2), see (3.4) and (3.5).

Adopting (3.10),

$$\Lambda_{sat}^2(W^2) = C_1 \left(\frac{W^2}{1\text{GeV}^2}\right)^{C_2}, \quad W^2 = \frac{Q^2}{x}, \quad (7.3)$$

the low- $x$  scaling variable  $\eta(W^2, Q^2)$  from (3.8), expressed in terms of the parton variables  $x$  and  $Q^2$ , becomes

$$\eta \equiv \eta(W^2 = \frac{Q^2}{x}, Q^2) = \frac{x^{C_2} (Q^2 + m_0^2)}{C_1 (Q^2)^{C_2}}, \quad (7.4)$$

and  $\mu(W^2)$  from (3.9) is given by

$$\mu \equiv \mu(W^2 = \frac{Q^2}{x}) = \frac{x^{C_2}}{C_1} \frac{m_0^2}{(Q^2)^{C_2}}. \quad (7.5)$$

The numerical value of the exponent  $C_2$ , for a given value of  $\rho$  is fixed by the large- $Q^2$  constraint (6.9).

Turning to the examination of the validity of the evolution equation for  $F_2(x, Q^2)$  in the form of the first equality in (6.6) relating the logarithmic derivative of  $F_2(x, Q^2)$  to the longitudinal structure function  $F_L(x, Q^2)$ , we introduce the ratio

$$\begin{aligned} \text{Ratio} &\equiv \frac{\frac{\partial F_2(x, Q^2)}{\partial \ln Q^2}}{F_L\left(\frac{\xi_L}{\xi_2} x, Q^2\right)} \\ &= 1 + \Delta\left(\eta\left(W^2 = \frac{Q^2}{x}, Q^2\right), \mu\left(W^2 = \frac{Q^2}{x}\right)\right), \end{aligned} \quad (7.6)$$

where, according to the validity of (6.6) under constraint (6.9), we have  $\Delta(\eta, \mu) \cong 0$  for sufficiently large  $Q^2 \gtrsim 10\text{GeV}^2$ . Deviations from the validity of the evolution equation (6.5) are accordingly parametrized by  $\Delta(\eta, \mu)$  according to (7.6).

Note that  $\Delta(\eta, \mu) \neq 0$  in (7.6) may be due to either a consequence of a violation of the evolution equation (6.5), under validity of the relation between the gluon distribution and the longitudinal structure function (2.8), or else to a violation of (2.8), not excluding both cases simultaneously. In any case,  $\Delta(\eta, \mu) \neq 0$  implies violation of the underlying parton model. At low  $\eta$ , the interaction is dominantly due to the interaction of low-lying  $q\bar{q}$  vector states with the gluon field in the proton, or, equivalently (see(2.6)) to the interaction of the photon with low-lying  $q\bar{q}$  vector states and not with freely moving quarks and gluons. Nevertheless, one may formally define a gluon distribution function according to (2.9) and (3.32).

From (7.1), the derivative of  $F_2(x, Q^2)$  is obtained as

$$\begin{aligned} \frac{\partial F_2(x, Q^2)}{\partial \ln Q^2} &= \frac{Q^2}{4\pi^2\alpha} \frac{\sigma_{\gamma p}(W^2)}{\ln \frac{\rho}{\mu(W^2)}} \left[ \left( I_T^{(1)} \left( \frac{\eta}{\rho}, \frac{\mu}{\rho} \right) + I_L^{(1)}(\eta, \mu) \right) \right. \\ &\quad \times \left( 1 + \frac{\ln \frac{\rho}{\mu(W^2)}}{\sigma_{\gamma p}(W^2)} \frac{\partial}{\partial \ln W^2} \frac{\sigma_{\gamma p}(W^2)}{\ln \frac{\rho}{\mu(W^2)}} \right) \\ &\quad \left. + \frac{\partial}{\partial \ln Q^2} \left( I_T^{(1)} \left( \frac{\eta}{\rho}, \frac{\mu}{\rho} \right) + I_L^{(1)}(\eta, \mu) \right) \right], \quad (7.7) \end{aligned}$$

and the denominator of (7.6) is given by

$$F_L \left( \frac{\xi_L}{\xi_2} x, Q^2 \right) = \frac{Q^2}{4\pi^2\alpha} \frac{\sigma_{\gamma p} \left( \frac{\xi_2}{\xi_L} W^2 \right)}{\ln \frac{\rho}{\mu \left( \frac{\xi_2}{\xi_L} W^2 \right)}} I_L^{(1)} \left( \frac{\xi_L}{\xi_2} \eta, \frac{\xi_L}{\xi_2} \mu \right). \quad (7.8)$$

In connection with the derivatives appearing in (7.7), we mention the equality  $\frac{\partial}{\partial \ln W^2} = \frac{\partial}{\partial \ln Q^2}$ , and moreover, we note the derivatives

$$\begin{aligned} Q^2 \frac{\partial \eta}{\partial Q^2} &= (1 - C_2)\eta - \mu, \\ Q^2 \frac{\partial \mu}{\partial Q^2} &= -C_2\mu. \end{aligned} \quad (7.9)$$

Since  $\sigma_{\gamma p}(W^2)$  only weakly depends on  $W^2$ , one may approximate “Ratio” defined in (7.6) by ignoring the derivative of  $\sigma_{\gamma p}(W^2)$  in (7.7). Explicitly, Ratio from (7.6) becomes<sup>10</sup>

$$\begin{aligned} \text{Ratio} &= \frac{1}{I_L^{(1)} \left( \frac{\xi_L}{\xi_2} \eta, \frac{\xi_L}{\xi_2} \mu \right)} \\ &\quad \times \left[ I_T^{(1)} \left( \frac{\eta}{\rho}, \frac{\mu}{\rho} \right) + I_L^{(1)}(\eta, \mu) \right. \\ &\quad \left. + \frac{\partial}{\partial \ln Q^2} \left( I_T^{(1)} \left( \frac{\eta}{\rho}, \frac{\mu}{\rho} \right) + I_L^{(1)}(\eta, \mu) \right) \right] \\ &= \frac{1}{I_L^{(1)} \left( \frac{\xi_L}{\xi_2} \eta, \frac{\xi_L}{\xi_2} \mu \right)} \times \left[ I_T^{(1)} \left( \frac{\eta}{\rho}, \frac{\mu}{\rho} \right) + I_L^{(1)}(\eta, \mu) \right. \\ &\quad \left. + [(1 - C_2)\eta - \mu] \frac{\partial}{\partial \eta} \left( I_T^{(1)} \left( \frac{\eta}{\rho}, \frac{\mu}{\rho} \right) + I_L^{(1)}(\eta, \mu) \right) \right]. \end{aligned} \quad (7.10)$$

Moreover, since  $\mu(W^2) = m_0^2/\Lambda_{sat}^2(W^2)$ , with  $m_0^2 = 0.15\text{GeV}^2$ , for sufficiently large  $W^2$ ,  $\mu(W^2)$  is small compared to unity,  $\mu(W^2) \ll 1$ , and the approximation of  $I_L^{(1)}$  and  $I_T^{(1)}$  in terms of  $I_0(\eta)$  [15] given by (A3) to (A5) in Appendix A may be inserted when numerically evaluating Ratio in (7.6) and (7.10).

Making use of

$$\frac{d}{d\eta} I_0(\eta) = \frac{-2}{1 + 4\eta} \left( I_0(\eta) - \frac{1}{2\eta} \right) \quad (7.11)$$

<sup>10</sup> In (7.10), the shift  $\xi_2/\xi_L W^2$  in  $\sigma_{\gamma p} \left( \frac{\xi_2}{\xi_L} W^2 \right) / \ln \frac{\rho}{\mu \left( \frac{\xi_2}{\xi_L} W^2 \right)}$  from (7.8) is ignored.

together with (7.9), Ratio in (7.10) becomes a function that depends on  $\eta$ ,  $\mu$  and  $I_0(\eta)$ . The different dependence of  $I_0(\eta)$  on  $\eta$  at large  $\eta \gg 1$ , where

$$I_0(\eta) \cong \frac{1}{2\eta} \left( 1 - \frac{1}{6\eta} \right) + O \left( \frac{1}{\eta^3} \right), \quad (7.12)$$

and at small  $\eta$  of  $\mu \leq \eta \ll 1$ , where

$$I_0(\eta) \cong \ln \frac{1}{\eta} \left( 1 - 2\eta \left( 1 - \frac{1}{\ln \frac{1}{\eta}} \right) \right) + \dots, \quad (7.13)$$

determines the different behavior of the numerical results for Ratio to be presented next.

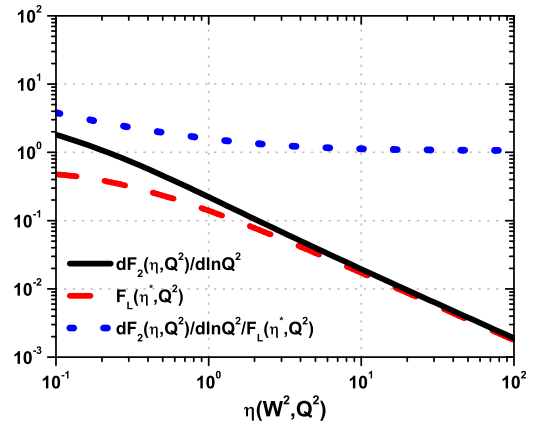


FIG. 11. The derivative of the structure function  $F_2(\eta(W^2 = Q^2/x), Q^2)$  and the longitudinal structure function  $F_L(\eta^* = (\xi_L/\xi_2)^{C_2} \eta, Q^2)$  together with the ratio of both of them. The results are based on evaluating (7.7) and (7.8).

For the numerical evaluation of Ratio from (7.6) with (7.7) and (7.8) inserted, and of Ratio explicitly given in (7.10), we use the parameters<sup>11</sup>

$$\rho = \frac{4}{3}, \quad C_2 = 0.29, \quad C_1 = 0.31 \text{ GeV}^2, \quad m_0^2 = 0.15 \text{ GeV}^2. \quad (7.14)$$

We also note  $\xi_L = 0.4$  (see (2.8)) and  $\xi_2 = 0.5$  (see (6.5)).

<sup>11</sup> We add the comment that only the value of  $C_1 = 0.31 \text{ GeV}^2$  is an entirely free fit parameter, whereas  $\rho = \frac{4}{3}$  is a consequence of the enhanced transverse size of  $q\bar{q}$  states originating from transversely relative to longitudinally polarized photons, and the exponent  $C_2 = 0.29$  is accordingly fixed by (6.9). The value of  $m_0^2 = 0.15 \text{ GeV}^2 < m_\rho^2$  is the starting point of the effective  $q\bar{q}$  continuum, including the  $\rho^0, \omega, \phi$  peaks. We add the remark that  $\sqrt{31} \text{ GeV} \cong 0.75 \text{ GeV}$  may be associated with the level spacing between the vector mesons  $\rho^0$  and  $\rho^0$ .

In Fig. 11, we show the derivative of the structure function as well as the longitudinal structure function according to (7.7) and (7.8) respectively, and their ratio defined by (7.6). For  $W^2$ , the value of  $W^2 = 10^5 \text{ GeV}^2$  was used <sup>12</sup>.

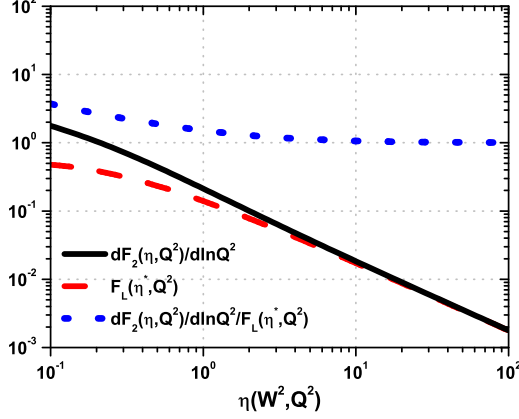


FIG. 12. As Fig. 11, however using the approximation  $\sigma_{\gamma p}(W^2) \cong \text{const}$ , compare to (7.10).

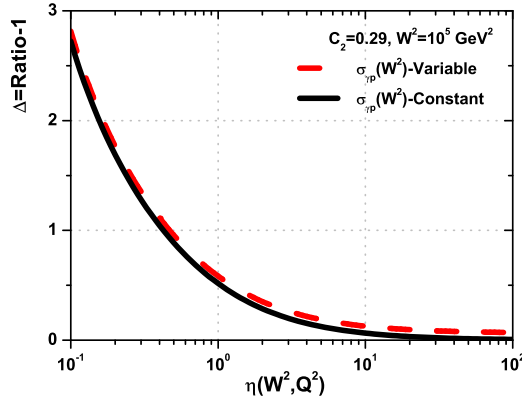


FIG. 13. The deviation from validity of the evolution equation obtained according to Figs. 11 and 12, respectively.

Since  $\sigma_{\gamma p}(W^2)$  depends weakly on  $W^2$ , we expect the numerical results of Fig. 11 not being drastically affected, if in (7.7) the term proportional to the derivative of  $\sigma_{\gamma p}(W^2)$  is put to zero. The corresponding value of Ratio is explicitly given by (7.10). Comparison of the

results in Fig. 12 with the ones in Fig. 11 indeed confirms that Ratio can reliably be evaluated according to the simple expression (7.10) upon insertion of  $I_T^{(1)}$  and  $I_L^{(1)}$  from (A.3) to (A.5).

In Fig. 13, we show the deviation  $\Delta(\eta(W^2 = \frac{Q^2}{x}), \mu(W^2))$  of Ratio in (7.6) from unity on a linear scale. Remember, a value of unity means strict validity of the first DGLAP evolution equation (6.1) in the approximation (6.4) and (6.5). A deviation smaller than  $\Delta(\eta(W^2 = \frac{Q^2}{x}), \mu(W^2)) \cong 0.1$  to 0.2 according to Fig. 13 requires  $\eta(W^2, Q^2) \gtrsim 5$ . The weaker increase of  $F_L(\eta(x, Q^2), Q^2)$  relative to the derivative of  $F_2(\eta(x, Q^2), Q^2)$  with decreasing  $\eta(x, Q^2)$ , or decreasing  $x$  at fixed  $Q^2$ , see (7.4), implies the substantial violation of the evolution equation reaching  $\Delta(\eta(W^2, Q^2), \mu(W^2)) \cong 2.7$  at  $\eta(W^2, Q^2) \cong 0.1$ .

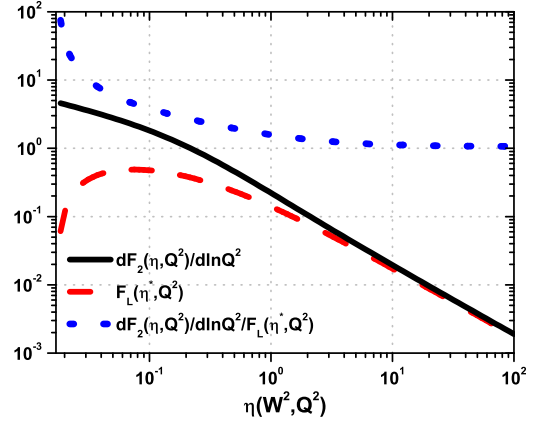


FIG. 14. The extension of Fig. 11 to the  $Q^2 \rightarrow 0$  limit of  $\eta(W^2, Q^2) \rightarrow \mu(W^2)$  for  $W^2 = 10^5 \text{ GeV}^2$

Fig. 14 explicitly shows that the increase of Ratio relative to unity with decreasing  $\eta$  is strongly correlated to the necessary vanishing of the longitudinal structure function,  $F_L(\eta(W^2, Q^2), \mu(W^2))$ , in the denominator of Ratio in the limit of  $\eta(W^2, Q^2) \rightarrow \mu(W^2)$  for  $Q^2 \rightarrow 0$ .

The value of  $\eta \cong 5$  quantifies the region in the  $(Q^2, x)$  plane, see Fig. 15, below which the evolution equation becomes violated. It is amusing to note the coincidence of this value with the value of  $\eta \cong 5$ , where the behavior of  $\sigma_{\gamma^* p} \sim 1/\eta$  of the CDP in Fig. 1 turns from the region of color transparency to the region of hadronlike behavior. Above  $\eta \cong 5$ , we have pQCD-evolution or CDP-color-transparency, while below  $\eta \cong 5$ , we have a violation of conventional evolution that is equivalent to hadronlike saturation.

In terms of  $x$  and  $Q^2$ , according to Fig. 15, at fixed value  $Q^2$  with decreasing  $x$ , or at fixed value of  $x$  with decreasing  $Q^2$ , the region of hadronlike behavior is reached

<sup>12</sup> As a consequence of the dominant dependence on  $\eta(W^2, Q^2)$ , the absolute value of  $W^2$  is only relevant with respect to  $\sigma_{\gamma p}(W^2)$  and  $\mu(W^2)$  in (7.7) and (7.8).

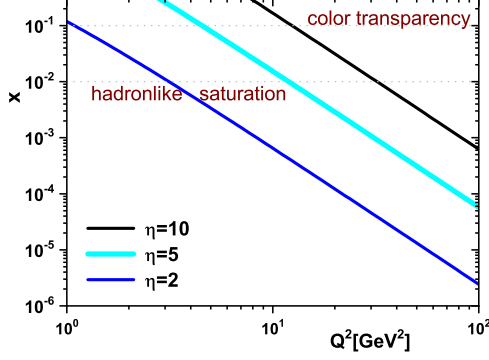


FIG. 15. The  $(Q^2, x)$  plane, showing the regions of  $\eta(W^2, Q^2) > 5$  (approximate validity of conventional evolution) with  $\Delta(\eta, \mu) \cong 0$ , and of  $\eta(W^2, Q^2) < 5$ , where  $\Delta(\eta, \mu) \neq 0$  occurs.

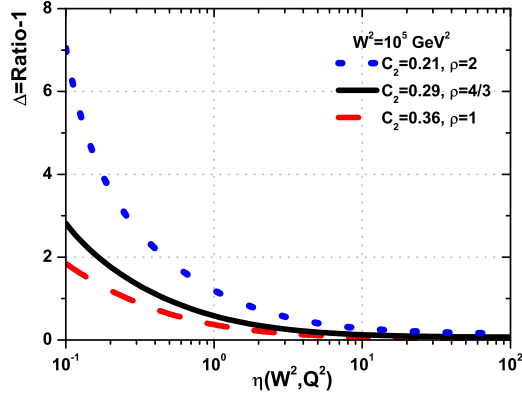


FIG. 16. The effect of the variation of  $\rho$ .

that in connected with a violation of standard evolution.

In Fig. 16, we address the question of the dependence of the above conclusion on the value of  $\rho$  that specifies the asymptotic behavior of the longitudinal-to-transverse ratio in photoabsorption via  $R = 1/2\rho$ . As long as precision experimental data on  $R$ , and accordingly on  $\rho$ , are lacking, it is interesting to vary  $\rho$  around its preferred value of  $\rho = 4/3$ , implying different values of the exponent  $C_2$  according to (6.9). From Fig. 16, we infer that a change of  $\rho$  does qualitatively not significantly change our general conclusion obtained for  $\Delta(\eta(W^2 = Q^2/x), Q^2)$ .

In Fig. 17, we show Ratio according to (7.10) as a function of  $Q^2$  at fixed  $x$ , upon replacing  $\eta$  and  $\mu$  in terms of  $x$  and  $Q^2$  according to (7.4) and (7.5). The figure shows for decreasing fixed values of  $x$  the increasingly stronger deviation of Ratio from Ratio=1 with decreasing  $Q^2$ .

In Figs. 11 to 14, we showed Ratio from (7.6) as a function of  $\eta(W^2, Q^2)$ . In connection with the extraction

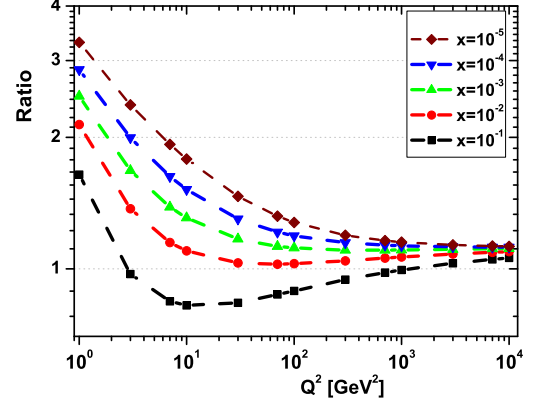


FIG. 17. The Ratio (7.6) as a function of  $Q^2$  in a wide range of  $x$ ,  $x = 10^{-5} \dots 10^{-1}$ .

of the gluon distribution from DIS experimental data, one frequently uses a fixed value of  $Q^2$ , chosen as low as  $Q^2 = 1.9 \text{ GeV}^2 \cong 2 \text{ GeV}^2$ , as starting scale for the evolution of the gluon distribution with increasing  $Q^2$  at fixed  $x$ .

TABLE III. Here  $\Delta = \text{Ratio} - 1$  and  $C_2 = 0.29$ .

$Q^2 [\text{GeV}^2]$	$x$	$W^2 [\text{GeV}^2]$	$\eta$	$\Delta + 1$	$\frac{1}{\Delta + 1}$
2	$10^{-2}$	$2.10^2$	1.492	1.544	0.648
2	$10^{-3}$	$2.10^3$	0.765	1.894	0.528
2	$10^{-4}$	$2.10^4$	0.392	2.252	0.444
2	$10^{-5}$	$2.10^5$	0.201	2.662	0.376
20	$10^{-2}$	$2.10^3$	7.172	1.041	0.961
20	$10^{-3}$	$2.10^4$	3.678	1.204	0.831
20	$10^{-4}$	$2.10^5$	1.886	1.362	0.734
20	$10^{-5}$	$2.10^6$	0.967	1.563	0.640
100	$10^{-2}$	$1.10^4$	22.351	1.026	0.975
100	$10^{-3}$	$1.10^5$	11.463	1.115	0.897
100	$10^{-4}$	$1.10^6$	5.879	1.189	0.841
100	$10^{-5}$	$1.10^7$	3.015	1.277	0.783

In Table III, we show the results for  $(1 + \Delta)^{-1}$  according to (7.6) with (7.7) and (7.8) for fixed  $Q^2 = 2 \text{ GeV}^2$  and the typical range of  $10^{-2} \leq x \leq 10^{-5}$ , corresponding to an interval of  $\eta$  approximately given by  $1.5 \geq \eta \geq 0.2$ . According to Table III, we observe a dramatic correction factor to standard evolution of magnitude  $0.6 \geq (1 + \Delta)^{-1} \geq 0.4$ . This correction to evolution is due to a strong violation of the impulse approximation of the pQCD improved parton model at low  $Q^2$ . The associated transition to hadronlike  $(q\bar{q})p$  interactions is outside the range of validity of the standard evolution equations. It comes without surprise that global DIS

data fits based on imposing evolution from a low- $Q^2$ -starting input scale “do not describe the deep inelastic scattering data in the low- $x$ , low- $Q^2$  region very well”, see ref. [6].

In Table III, in addition to the choice of  $Q^2 = 2 \text{ GeV}^2$ , we also give the results for the correction factor  $(1+\Delta)^{-1}$  at  $Q^2 = 20 \text{ GeV}^2$ . For  $x = 10^{-2}$ , with  $(1+\Delta)^{-1} = 0.96 \cong 1$ , we have consistency with perturbative evolution, as expected. For sufficiently large  $W^2$ , or  $10^{-3} > x > 10^{-5}$ , we observe the expected transition from unmodified pQCD evolution to hadronlike saturation.

We turn to the discussion of the gluon distribution function. Rewriting (7.6), and substituting the gluon distribution from (2.9), we find

$$\begin{aligned} \frac{\partial F_2(x, Q^2)}{1 + \Delta(\eta, \mu)} &= F_L\left(\frac{\xi_L}{\xi_2} x, Q^2\right) \\ &= \frac{\alpha_s(Q^2)}{9\pi} R_{e^+e^-} G\left(\frac{x}{\xi_2}, Q^2\right), \end{aligned} \quad (7.15)$$

where  $R_{e^+e^-} = 10/3$  for four flavors of quarks. The factor  $(1+\Delta)^{-1}$  in (7.15), for  $\Delta \neq 0$  represents a violation of, or alternatively, a correction to the evolution equation for the gluon distribution with decreasing  $\eta$  for  $\eta(W^2 = Q^2/x, Q^2) \lesssim 5$ .

The violation of the evolution with decreasing  $Q^2$  may be seen directly in terms of the gluon distribution by showing the gluon distribution as a function of  $x$  for e.g.  $Q^2 = 100 \text{ GeV}^2$  and  $Q^2 = 2 \text{ GeV}^2$  i.e. rewriting (7.15) as

$$G(x, Q^2) = \frac{\frac{\partial F_2(\xi_2 x, Q^2)}{\partial \ln Q^2}}{1 + \Delta(\eta, \mu)} \frac{9\pi}{\alpha_s(Q^2) R_{e^+e^-}}, \quad (7.16)$$

where  $\Delta(\eta, \mu)$  is inserted from (7.6). In Fig.18 we show the gluon distribution according to (7.16). In addition, we show the gluon distribution under the ad hoc assumption of  $\Delta(\eta, \mu) \equiv 0$  corresponding to validity of evolution in violation of the CDP result where  $\Delta(\eta, \mu) \neq 0$ .

Fig.18 confirms our previous conclusion that the experimental data described by the CDP obey evolution at  $Q^2$  large,  $Q^2 \cong 100 \text{ GeV}^2$ , while evolution is violated at low  $Q^2$ , i.e., specifically for  $Q^2 = 1.9 \text{ GeV}^2$ . Since the experimental data violate the evolution equation at low  $Q^2$ , the assumption of a universal validity of the evolution equation at low  $Q^2$  is excluded. Relying on the universal absolute validity of the evolution equation at a low- $Q^2$  input scale in e.g. global fits to the experimental data is highly questionable.

The Ratio may be explicitly interpreted as a modification of the evolution equation (6.6). Upon substitution

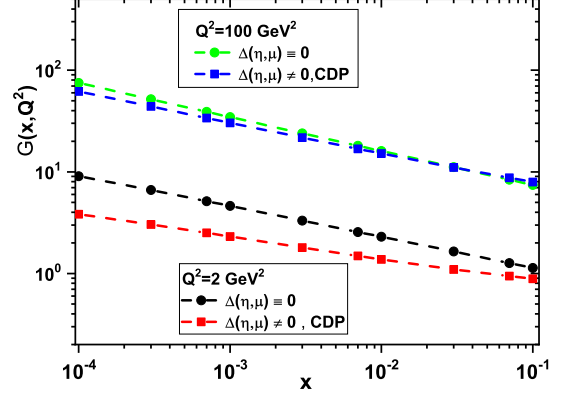


FIG. 18. The gluon distribution  $G(x, Q^2)$  deduced from Eq.(7.16) for  $\Delta(\eta, \mu) \neq 0$  and  $\Delta(\eta, \mu) \equiv 0$ .

of (7.10) equation (6.6) becomes

$$\begin{aligned} \frac{\partial F_2(x, Q^2)}{\partial \ln Q^2} &= F_L\left(\frac{\xi_L}{\xi_2} x, Q^2\right) \times \text{Ratio} \\ &= F_L\left(\frac{\xi_L}{\xi_2} x, Q^2\right) \frac{1}{I_L^{(1)}\left(\frac{\xi_L}{\xi_2} \eta, \frac{\xi_L}{\xi_2} \mu\right)} \\ &\quad \times \left[ I_T^{(1)}\left(\frac{\eta}{\rho}, \frac{\mu}{\rho}\right) + I_L^{(1)}(\eta, \mu) \right. \\ &\quad \left. + \frac{\partial}{\partial \ln Q^2} \left( I_T^{(1)}\left(\frac{\eta}{\rho}, \frac{\mu}{\rho}\right) + I_L^{(1)}(\eta, \mu) \right) \right], \end{aligned} \quad (7.17)$$

where the simple equations for  $I_{L,T}^{(1)}$  in Appendix (A3) to (A5) are to be inserted. At small  $\mu$ , the CDP evolution equation (7.17) becomes

$$\begin{aligned} \frac{\partial F_2(x, Q^2)}{\partial \ln Q^2} &\simeq F_L\left(\frac{\xi_L}{\xi_2} x, Q^2\right) \\ &\times \left\{ \frac{I_0(\eta) - \frac{(1-C_2)\eta}{1+4\eta} (2I_0(\eta) + \frac{1}{\eta})}{1-2\eta^* I_0(\eta^*)} \right\} \end{aligned} \quad (7.18)$$

where  $I_0$  is defined in (A.5). The factor multiplying the longitudinal structure function continuously converges towards unity at large  $Q^2$ . We note that the CDP evolution equation (7.17), differs from an ad hoc modification of conventional evolution, since it is an analytically determined smooth extrapolation to low  $Q^2$  consistent with DIS measurements.

## VIII. CONCLUSIONS.

Employing the pQCD relation between the longitudinal proton structure function and the gluon distribution function allows one to define a gluon distribution associated with the proton structure functions of the CDP at low  $x$  and any  $Q^2 \geq 0$ . The CDP gluon distribution depends on  $W^2 = Q^2/x$  and  $Q^2$ . For  $Q^2$  sufficient large ( $10 \text{ GeV}^2 \lesssim Q^2 \lesssim 100 \text{ GeV}^2$  at presently available energies)



the CDP gluon distribution, multiplied by  $\alpha_s(Q^2)$ , converges towards the asymptotic limit proportional to the saturation scale  $\Lambda_{\text{sat}}^2(W^2) = (\frac{W^2}{1\text{GeV}^2})^{C_2=0.29}$ .

Concerning evolution, the dependence of the logarithmic derivative of the parton structure function on  $x$  and  $Q^2$ , we find a CDP evolution equation that agrees with the standard model evolution equation in the limit of large  $Q^2$  at fixed low  $x$ .

At low  $Q^2$ , where photoabsorption cross section becomes hadronlike, the CDP evolution differs significantly from the standard one by an explicitly analytically given factor. Relying on a universal validity of the parton model and standard evolution at a low- $Q^2$  input scale, such as  $Q^2 \cong 1.9 \text{ GeV}^2$ , as frequently employed in global fits, is accordingly highly questionable and should be excluded.

## APPENDIX A

The explicit expressions for the functions  $I_{L,T}^{(1)}(\eta(W^2, Q^2), \mu(W^2))$  in (3.2) are given by:

$$I_{L,T}(\eta(W^2, Q^2), \mu(W^2)) = I_{L,T}^{(1)}(\eta(W^2, Q^2), \mu(W^2)) \times (1 + 0(\mu(W^2))), \quad (\text{A.1})$$

where  $I_L^{(1)}(\eta(W^2, Q^2), \mu(W^2))$  and  $I_T^{(1)}(\eta(W^2, Q^2), \mu(W^2))$  are given by

$$\begin{aligned} I_L^{(1)}(\eta, \mu) &= \frac{\eta - \mu}{\eta} \\ &\times \left( 1 - \frac{\eta}{\sqrt{1 + 4(\eta - \mu)}} \right. \\ &\times \ln \frac{\eta(1 + \sqrt{1 + 4(\eta - \mu)})}{4\mu - 1 - 3\eta + \sqrt{(1 + 4(\eta - \mu))((1 + \eta)^2 - 4\mu)}} \Bigg), \\ I_T^{(1)}(\eta, \mu) &= \frac{1}{2} \ln \frac{\eta - 1 + \sqrt{(1 + \eta)^2 - 4\mu}}{2\eta} \\ &- \frac{\eta - \mu}{\eta} + \frac{1 + 2(\eta - \mu)}{2\sqrt{1 + 4(\eta - \mu)}} \\ &\times \ln \frac{\eta(1 + \sqrt{1 + 4(\eta - \mu)})}{4\mu - 1 - 3\eta + \sqrt{(1 + 4(\eta - \mu))((1 + \eta)^2 - 4\mu)}}. \end{aligned} \quad (\text{A.2})$$

For  $\mu(W^2) \ll 1$  (and  $\eta(W^2, Q^2) \geq \mu(W^2)$ ) the functions  $I_L^{(1)}(\eta, \mu)$  and  $I_T^{(1)}(\eta, \mu)$  can be simplified to become

$$I_L^{(1)}(\eta, \mu) = \frac{\eta - \mu}{\eta} (1 - 2\eta I_0(\eta)) \quad (\text{A.3})$$

and

$$I_T^{(1)}(\eta, \mu) = I_0(\eta) - \frac{\eta - \mu}{\eta} (1 - 2\eta I_0(\eta)), \quad (\text{A.4})$$

where

$$I_0(\eta) = \frac{1}{\sqrt{1 + 4\eta}} \ln \frac{\sqrt{1 + 4\eta} + 1}{\sqrt{1 + 4\eta} - 1}. \quad (\text{A.5})$$

We also note that for the relevant range of  $\eta \gg \mu$ , or  $Q^2 \gg m_0^2$ , we may put  $\mu = 0$  in (A.3) and (A.4).

## APPENDIX B

In this Appendix we show the coefficients of the structure functions  $F_2(x, Q^2)$  given in (4.1) as taken from ref. [22]. The coefficients in (4.1),

$$\begin{aligned} A(Q^2) &= a_0 + a_1 \ln \left( 1 + \frac{Q^2}{\mu^2} \right) + a_2 \ln^2 \left( 1 + \frac{Q^2}{\mu^2} \right), \\ B(Q^2) &= b_0 + b_1 \ln \left( 1 + \frac{Q^2}{\mu^2} \right) + b_2 \ln^2 \left( 1 + \frac{Q^2}{\mu^2} \right), \\ C(Q^2) &= c_0 + c_1 \ln \left( 1 + \frac{Q^2}{\mu^2} \right), \\ D(Q^2) &= \frac{Q^2(Q^2 + \lambda M^2)}{(Q^2 + M^2)^2}, \end{aligned}$$

depend on the fit parameters listed in Table II.

TABLE B.1. The effective parameters at low  $x$  for  $0.15\text{GeV}^2 < Q^2 < 3000\text{GeV}^2$  provided by the following values. The fixed parameters are defined by the Block-Halzen fit to the real photon-proton cross sections as  $M^2 = 0.753 \pm 0.068 \text{ GeV}^2$ ,  $\mu^2 = 2.82 \pm 0.290 \text{ GeV}^2$  and  $c_0 = 0.255 \pm 0.016$ .

parameters	value
$a_0$	$8.205 \times 10^{-4} \pm 4.62 \times 10^{-4}$
$a_1$	$-5.148 \times 10^{-2} \pm 8.19 \times 10^{-3}$
$a_2$	$-4.725 \times 10^{-3} \pm 1.01 \times 10^{-3}$
$b_0$	$2.217 \times 10^{-3} \pm 1.42 \times 10^{-4}$
$b_1$	$1.244 \times 10^{-2} \pm 8.56 \times 10^{-4}$
$b_2$	$5.958 \times 10^{-4} \pm 2.32 \times 10^{-4}$
$c_1$	$1.475 \times 10^{-1} \pm 3.025 \times 10^{-2}$
$n$	$11.49 \pm 0.99$
$\lambda$	$2.430 \pm 0.153$
$\chi^2$ (goodness of fit)	0.95



- 
- [1] L.A. Harland-Lang, A.D. Martin, P. Motylinski and R.S. Thorne, *Eur. Phys. J. C* **75**, 204 (2015).
- [2] S. Dulat et al., *Phys. Rev. D* **93**, no. 3, 033006 (2016).
- [3] R.D. Ball et al. [NNPDF Collaboration], *Eur. Phys. J. C* **77**, 663 (2017)
- [4] A. Buckley, J. Ferrando, S. Lloyd, K. Nordstrom, B. Page, M. Ruefenacht, M. Schoenherr and G. Watt, *Eur. Phys. J. C* **75**, 132 (2015).
- [5] H. Abramowicz et al. [H1 and ZEUS Collaborations], *Eur. Phys. J. C* **75**, 580 (2015).
- [6] M.R. Pelicer et al., *Eur. Phys. J. C* **79**, 9 (2019).
- [7] L.A. Harland-Lang, A.D. Martin, P. Motylinski and R.S. Thorne, *Eur. Phys. J. C* **76**, 186 (2016)
- [8] I. Abt, A.M. Cooper-Sarkar, B. Foster, V. Myronenko, K. Wichmann, M. Wing, *Phys. Rev. D* **94**, 034032 (2016).
- [9] L.N. Lipatov, *Sov. J. Nucl. Phys.* **20**, 94 (1975);  
V.N. Gribov, L.N. Lipatov, *Sov. J. Nucl. Phys.* **15**, 438 (1972);  
G. Altarelli, G. Parisi, *Nucl. Phys. B* **126**, 298 (1977);  
Yu.L. Dokshitzer, *Sov. Phys. JETP* **46**, 641 (1977).
- [10] L.V. Gribov, E.M. Levin and M.G. Ryskin, *Phys. Rept.* **100**, 1 (1983).
- [11] A.H. Mueller and J.-W. Qiu, *Nucl. Phys. B* **268**, 427 (1986).
- [12] G. Cvetič, D. Schildknecht, A. Shoshi, *Eur. Phys. J. C* **13**, 301 (2000)
- [13] D. Schildknecht, *Nucl. Phys. B (Proc. Suppl.)* **99**, 121 (2001);  
D. Schildknecht, B. Surrow, M. Tentyukov, *Phys. Lett. B* **499**, 116 (2001);  
G. Cvetič, D. Schildknecht, B. Surrow, M. Tentyukov, *Eur. Phys. J. C* **20**, 77 (2001);  
N.N.Nikolaev and B.G.Zakharov, *Z.Phys.C* **49**, 607 (1991).
- [14] M. Kuroda and D. Schildknecht, *Phys. Rev. D* **85**, 094001 (2011).
- [15] M. Kuroda and D. Schildknecht, *Int. J. of Mod. Phys. A* **31**, 1650157 (2016).
- [16] J.J. Sakurai and D. Schildknecht, *Phys. Lett.* **40B**, 121 (1972);  
B. Gorczyca and D. Schildknecht, *Phys. Lett.* **47B**, 71 (1973);  
H. Fraas, B.J. Read and D. Schildknecht, *Nucl. Phys. B* **86**, 346 (1975);  
R. Devenish and D. Schildknecht, *Phys. Rev. D* **14**, 93 (1976).
- [17] D. Schildknecht, *Acta Physica Polonica* **B37**, 595 (2006).
- [18] M.Kuroda and D.Schildknecht, *Phys.Rev.D* **96**, 094013 (2017).
- [19] G. Altarelli, G. Martinelli, *Phys. Lett. B* **76**, 89 (1978);  
A.D. Martin et al., *Phys. Rev. D* **37**, 1161 (1988);  
A.M. Cooper-Sarkar et al., *Z. Phys. C* **39**, 281 (1988);  
A.M. Cooper-Sarkar et al., *Acta Phys. Pol. B* **34**, 2911 (2003);  
R.G. Roberts, *The Structure of the Proton*, (Cambridge University Press 1990).
- [20] D.Schildknecht, *Phys.Rev.D***104**, 014009 (2021).
- [21] Particle Data Group, *Phys. Rev. D* **86**, 1 (2012).
- [22] M.M. Block, L. Durand and P. Ha, *Phys. Rev. D* **89**, 094027 (2014).
- [23] M. Froissart, *Phys. Rev.* **123**, 1053 (1961).
- [24] M.Kuroda and D.Schildknecht, *Phys.Lett.B* **670**, 129 (2008).
- [25] M.M. Block, L. Durand and Douglas W. McKay, *Phys. Rev. D* **77**, 094003 (2008).
- [26] M.M. Block and L. Durand, *arXiv [hep-ph]: 0902.0372* (2009).
- [27] K. Prytz, *Phys. Lett. B* **311**, 286 (1993).